Physica E: Low-dimensional Systems and Nanostructures 96 (2018) 46–53

Contents lists available at ScienceDirect

Physica E: Low-dimensional Systems and Nanostructures

journal homepage: www.elsevier.com/locate/physe

Spurious heat conduction behavior of finite-size graphene nanoribbon under extreme uniaxial strain caused by the AIREBO potential

Xueming Yang [a,b,*], Sihan Wu [a], Jiangxin Xu [a], Bingyang Cao [b,**], Albert C. To [c]

[a] Department of Power Engineering, North China Electric Power University, Baoding 071003, China
[b] Key Laboratory for Thermal Science and Power Engineering of Ministry of Education, Department of Engineering Mechanics, Tsinghua University, Beijing 100084, China
[c] Department of Mechanical Engineering and Materials Science, University of Pittsburgh, PA 15260, USA

ARTICLE INFO

Keywords:
Graphene
Nanoribbons
Thermal conductivity
Molecular dynamics simulations

ABSTRACT

Although the AIREBO potential can well describe the mechanical and thermal transport of the carbon nanostructures under normal conditions, previous studies have shown that it may overestimate the simulated mechanical properties of carbon nanostructures in extreme strains near fracture. It is still unknown whether such overestimation would also appear in the thermal transport of nanostructrues. In this paper, the mechanical and thermal transport of graphene nanoribbon under extreme deformation conditions are studied by MD simulations using both the original and modified AIREBO potential. Results show that the cutoff function of the original AIREBO potential produces an overestimation on thermal conductivity in extreme strains near fracture stage. Spurious heat conduction behavior appears, e.g., the thermal conductivity of GNRs does not monotonically decrease with increasing strain, and even shows a "V" shaped reversed and nonphysical trend. Phonon spectrum analysis show that it also results in an artificial blue shift of G peak and phonon stiffening of the optical phonon modes. The correlation between spurious heat conduction behavior and overestimation of mechanical properties near the fracture stage caused by the original AIREBO potential are explored and revealed.

1. Introduction

Strain effects on thermal conductivity have attracted lots of attention due to their applications from nanoscales to geophysical scales [1]. The graphene nanoribbons (GNRs) have been investigated extensively in their electrical, thermal, and mechanical properties in recent years [2–7]. By tuning the strain, the thermal conductivity of GNRs can be changed dynamically, thus could be used in applications of thermal smart materials and thermal rectifiers [8]. Therefore it is of great importance to understand the strain effects on thermal conductivity of GNRs. When investigating the origin and physical insight of strain-induced modification of thermal conductivity of carbon-based nanomaterials, interatomic potentials play a vital role in atomistic simulations. When predicting the nanomaterials properties, the reliability of the prediction by atomistic simulations depends on whether and how accurately the employed interatomic potentials can capture the essential physics and chemistry [9]. Most existing carbon potentials were developed and validated only focusing on the behavior of carbon nanomaterials under normal conditions, e. g., normal ambient pressure, temperature, strain and stress; however, there is no guarantee that they perform well under extreme conditions of high stress. Especially for highly distorted bonds and configurations, the application of empirical interatomic potential becomes an extrapolation and the results have to be treated with caution [10].

In the original AIREBO potential [11–13], a cutoff function is employed for the covalent interaction (the REBO term of AIREBO) for atom distance between 1.7 and 2.0 Å, which allows a user to simulate covalent bond formation and bond breaking. Although the original AIREBO potential, one of the most commonly used and accurate potential for C—C bond in carbon based nanostructures [14–16], e.g. graphene and carbon nanotubes, can describe the mechanical and thermal transport of the carbon nanostructures under normal conditions well. However, past works [17–19] have shown that it may produce an overestimation of mechanical properties of nanostructures in extreme strains near fracture. To the best of our knowledge, it is still unknown whether such an overestimation will appear and affect the thermal transport of carbon nanostructrues.

To answer this question, in this work, the mechanical behavior and thermal transport of GNRs are studied by MD simulations using both the

* Corresponding author. Department of Power Engineering, North China Electric Power University, Baoding 071003, China.
** Corresponding author.
E-mail addresses: ncepub@hotmail.com (X. Yang), caoby@tsinghua.edu.cn (B. Cao).

https://doi.org/10.1016/j.physe.2017.10.006
Received 21 September 2017; Accepted 10 October 2017
Available online 13 October 2017
1386-9477/© 2017 Elsevier B.V. All rights reserved.

original and modified AIREBO potential. Results show that the original AIREBO potential produces thermal transport artifacts under extreme deformation conditions, which results in seriously overestimated thermal conductivity for graphene nanoribbons. More importantly, it will cause some spurious phenomenon, e.g., spurious heat conduction behavior, artificial blue shift of G peak and phonon stiffening of the optical phonon modes.

2. Computational methods

MD simulations using the AIREBO potential are carried out using the LAMMPS package [20]. The potential consists of three terms,

$$E = \frac{1}{2}\sum_{i}\sum_{j\neq i}\left[E_{ij}^{REBO} + E_{ij}^{LJ} + \sum_{k\neq i,j}\sum_{l\neq i,j,k} E_{ijkl}^{TORSION}\right] \tag{1}$$

E_{ij}^{REBO} stands for the hydrocarbon REBO potential; E_{ij}^{LJ} includes long range interactions similar to standard Leonard–Jones potential; $\sum_{k\neq i,jl\neq i,j,k} E_{ijkl}^{TORSION}$ is an explicit 4-body potential that describes various dihedral angle preferences in hydrocarbon configurations. All three terms are included in our calculations. In both the repulsive term and the attractive term of E_{ij}^{REBO}, a switching (cutoff) function $f_c(r)$ is defined to limit the interaction among the nearest neighbors and represents the cutoff function that decreases monotonically from 1 to 0 as:

$$f_c(r) = \begin{cases} 1, & r < R_{\min} \\ \left\{1 + \cos\left[\dfrac{\pi(r - R_{\min})}{R_{\max} - R_{\min}}\right]\right\}\Big/2, & R_{\min} \le r \le R_{\max} \\ 0, & r > R_{\max} \end{cases} \tag{2}$$

where $R_{\min}$ = 1.7 Å and $R_{\max}$ = 2.0 Å in original AIREBO potential [20,21]. However the authors of the Brenner potential and REBO potential have mentioned that such a value of parameter $R_{\min}$ in the cutoff function will give unusually high bond forces without a physical basis as C—C bonds are stretched beyond 1.7 Å. Thus they suggested the cutoff distance $R_{\min}$ should be extended far beyond the inflection point [18] by setting $R_{\min}$ to be 2.0 while including C—C interactions only for those atom pairs that are less than 2.0 Å apart in the initial. Their suggestion indicates that the nearest-neighbor character of interactions should be preserved, and a bond list using the original cutoff distance (2 Å) is constructed for the initial system that was left unchanged during the simulations. By following their suggestions, the nonphysical failure mechanisms can be avoided, and results can give reasonable results for the fracture of carbon nanostructures; however, this modification is no longer capable of handling bond forming [22,23] and cannot handle some extreme cases, such as deriving carbon atomic chains from ultra-narrow graphene nanoribbons, carbon nanotubes or nanobuds [24–29]. Other researchers have attempted other cutoff distances $R_{\min}$ value, e.g. 1.9 [30], 1.92 [31,32], 1.95 [33,34] and 2.05 [35], and so on; however, we can see from the following that these $R_{\min}$ values are not guaranteed to fully avoid nonphysical failures to occur. Although more and more studies [14,36–39] have followed the suggestion in Ref. [18], there are more studies using the original AIREBO potential and $R_{\min}$ is still be set as 1.7 Å even in the newest version of LAMMPS package.

The (nominal) strain and the engineering (nominal) stress in the x direction are defined as

$$\varepsilon_x = \frac{l_x - l_x^0}{l_x^0}, \quad \sigma_x = \frac{1}{V^0}\frac{\partial U}{\partial \varepsilon_x} \tag{3}$$

where l_x^0 is the initial lengths of the GNRs in x (i.e. longitudinal) direction at zero strain, l_x is the strained lengths of the GNRs, U is the strain energy, $V^0 = l_x^0 S$ is the initial volume of the structure, and S is the effective cross-sectional area of the GNRs on which the tensile force is applied. The Young's modulus Y in the x direction is defined via the equation

$$Y = \frac{1}{V^0}\frac{\partial^2 U}{\partial \varepsilon_x^2}\bigg|_{\varepsilon_x=0} \tag{4}$$

The schematic of the simulation setup for calculating the mechanical properties of the GNRs in the tensile process is shown in Fig. 1(a). MD simulations are performed using the NVT ensemble at a temperature of 300 K. The blue part on the left of the system is fixed during the simulation, and displacement step is applied on the right blue part which is held rigid. All atoms except the end atoms are attached to the Nosé–Hoover thermostat during the loading process. Each displacement step is followed by 1000 relaxation steps, and simulation time step is set to be 0.5 fs. Such a simulation strategy has been recommended for MD simulations of the tensile loading process of the CNTs by Mylvaganam et al. [40]. The strain rates vary with length of GNRs in the range from 1.0×10^8 s^{-1} to 2×10^8 s^{-1} which is in agreement with the strain rates selected in Ref. [41].

The NEMD method is an approach based on the direct application of the Fourier law of heat conduction to predict the thermal conductivity. By imposing a heat flux and measuring the resulting temperature gradient, one can predict the thermal conductivity using the Fourier law:

$$q = -k\nabla T \tag{5}$$

where q is the heat flux vector, ∇T is the temperature gradient and k denotes the thermal conductivity.

The schematic of the simulation setup for calculating the thermal conductivity of the GNRs under different strains is shown in Fig. 1 (b), in which the fixed slabs, buffer slabs, hot slabs, and cold slabs are labeled. The atomistic coordinates of system at a specific strain can be successively extracted during a MD simulation of the tensile process. In the NEMD simulations, the left blue parts (fixed slabs) of the system is fixed rigidly, the applied heat flux method is used by adding/subtracting constant amount of kinetic energy to/from the hot/cold slab at a regular interval; the yellow parts (buffer slabs) between fixed and hot/cold slabs are in an attempt to reduce reflection of heat from the edge, and the gray part are free during simulation. In all the MD simulations, the initial length and width of armchair GNRs without tensile loading are 21.6 nm and 3.8 nm, and they are 20.6 nm and 4.06 nm for zigzag GNRs.

Here, free boundary condition was applied in in-plane direction in order to explore the heat conduction behavior of the finite sized GNRs, and periodic boundary condition is applied in the out-plane direction with 2.0 nm vacuum space on each side of the GNR. Each simulation for thermal conductivity calculation was run for 6,000,000 time steps, with the temperature profile averaged over the last 1,000,000 time steps. For these simulations, the time step was 0.5 fs, and the thickness of graphene is chosen as 0.142 nm [42–44], which is the length of the carbon–carbon bond length.

3. Simulation results and discussion

3.1. Tensile behavior of GNRs

The stress-strain curves of the armchair GNR and zigzag GNR are calculated and compared by using both the original AIREBO potential ($R_{\min}$ = 1.7 Å) and modified AIREBO potential ($R_{\min}$ = 1.92 Å and 2.0 Å) which are shown in Fig. 2 (a) and (b), respectively.

In both Fig. 2 (a) and (b), for case of $R_{\min}$ = 2.0 Å, the stress first increases linearly with the strain owing to the elastic response of the bonds, and then non-linear elasticity begins and continues up to a critical strain, which can be ascribed to the combined effect of bond elongation and bond angle variation. Finally, brittle fracture takes place as a result of bond rupture. However, for the cases of $R_{\min}$ = 1.7 Å or 1.92 Å, a nonphysical "Second Linearly Elastic Deformation (SLED)" [37] appears and indicates an overestimated stress and spurious high bond forces in

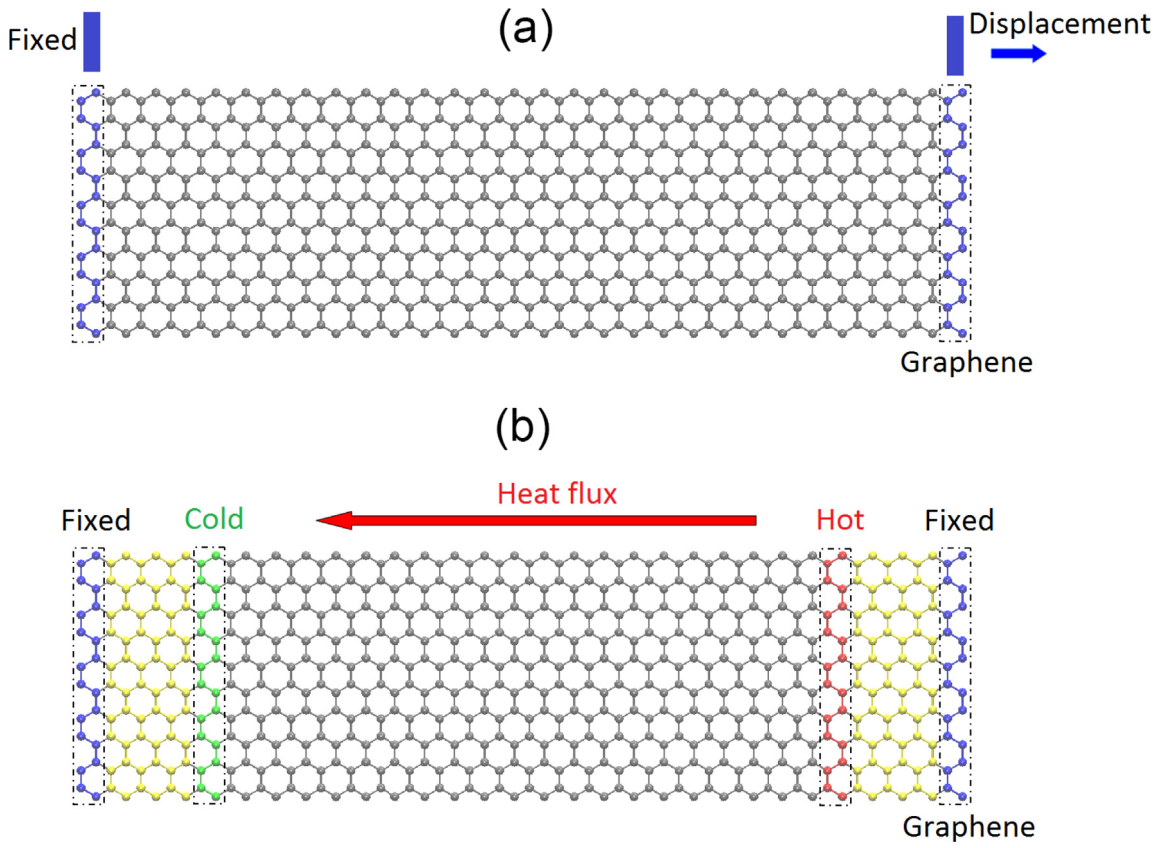

Fig. 1. Schematic diagram of the calculated GNRs. (a) for calculating the mechanical properties of the GNRs in the tensile process. (b) for calculating the thermal conductivity of the GNRs under different strains.

extreme strains near fracture. That also means the modification of setting $R_{min} = 1.92$ Å cannot guarantee the full avoidance of nonphysical failures and the overestimation of mechanical properties of nanostructures near the fracture stage during the tensile process. It also can be observed that finite-size GNRs under free boundary condition shows obvious fluctuations when temperatures are non-zero even their end atoms are fixed, and these fluctuations induced by temperature will result in initial stress in the GNRs before the tensile process start.

The modified AIREBO potential ($R_{min} = 2.0$ Å) can give reasonable results comparing with experimental results. Here the obtained Young's modulus is 1.02 TPa and 0.95 TPa in zigzag and armchair directions, which agrees well with the experimental result of 1.0 TPa [45]. The critical stresses for both the zigzag and armchair oriented graphene obtained from our simulations are 127.8 GPa and 85.6 GPa, respectively, which are in good agreement with the results obtained by MD simulations (121 GPa) [46] and by experiment (123.5 GPa) [45].

3.2. Thermal conductivity of GNRs under different strains

The thermal conductivity of the finite-size armchair GNRs and zigzag GNRs are calculated and compared by using both original AIREBO potential ($R_{min} = 1.7$ Å) and the modified AIREBO potential ($R_{min} = 1.92$ Å and 2.0 Å), as shown in Fig. 3 (a) and (b). For the armchair GNR (with a length of about 20 nm), the thermal conductivity obtained by our computational model at $\varepsilon = 0$ is 193 W/mK, respectively, which is close to previous simulated values of ~180 W/mK [47] (half length of GNRs is considered due to the RNEMD) and ~230 W/mK [48]. For the case of $R_{min} = 1.92$ Å, the obtained maximum strain is even large than that in the case of $R_{min} = 1.7$ Å as shown in Fig. 2 (a) and (b); however, the structures under large strain are not stable and will break when simulating heat conduction. As shown in Fig. 3(a) and (b), the results of thermal conductivity and their corresponding strain range is almost the same for the cases of $R_{min} = 2.0$ Å and $R_{min} = 1.92$ Å, and the valid strain for thermal conductivity of armchair GNRs and zigzag GNRs is 0.076 and 0.125 which are much less than the obtained maximum strain calculated by $R_{min} = 1.7$ Å.

Previous studies [44,49] have reported that the thermal conductivity of GNRs monotonically goes down with increasing strain. However, spurious heat conduction behavior appears in our calculations by the original AIREBO potential ($R_{min} = 1.7$ Å), and it can be observed from Fig. 3(a) and (b) that the thermal conductivity of GNRs does not monotonously decrease with increasing applied strain, and in the later stage of the tensile strain, thermal conductivity of GNRs shows a steady increase with applied strain. The obtained relation of the thermal conductivity k and strain ε does not follow the approximation, $k \sim T^{-1}\varepsilon^{-\gamma}$, proposed by Bhowmick[1]. Therefore, it can be concluded that thermal conductivity values of GNRs under tensile strain are significantly overestimated through the use of the original AIREBO potential in extreme strains near fracture, and even shows a "V" shaped reversed trend, which is nonphysical in nature.

3.3. Discussions

Why such an anomalous heat conduction behavior appears should be investigated. From the view of mechanics, the applied tensile strain will change the Young's modulus of GNRs, and consequently affect the thermal conductivity. The speed of sound can be denoted as $v = \sqrt{E/\rho}$, where E and ρ is the Young modulus and the mass density of GNRs. The square root of the nominal modulus derived through differentiation of the stress with respect to strain in Fig. 2(a) and (b) are shown as the red lines in Fig. 4(a) and (b), respectively. The green dots in Fig. 4 are corresponding to the strain of the scattered points in Fig. 3. The variation trend of the nominal modulus agree with that of the thermal conductivity well, thus demonstrated that the non-monotonic decrease of the thermal

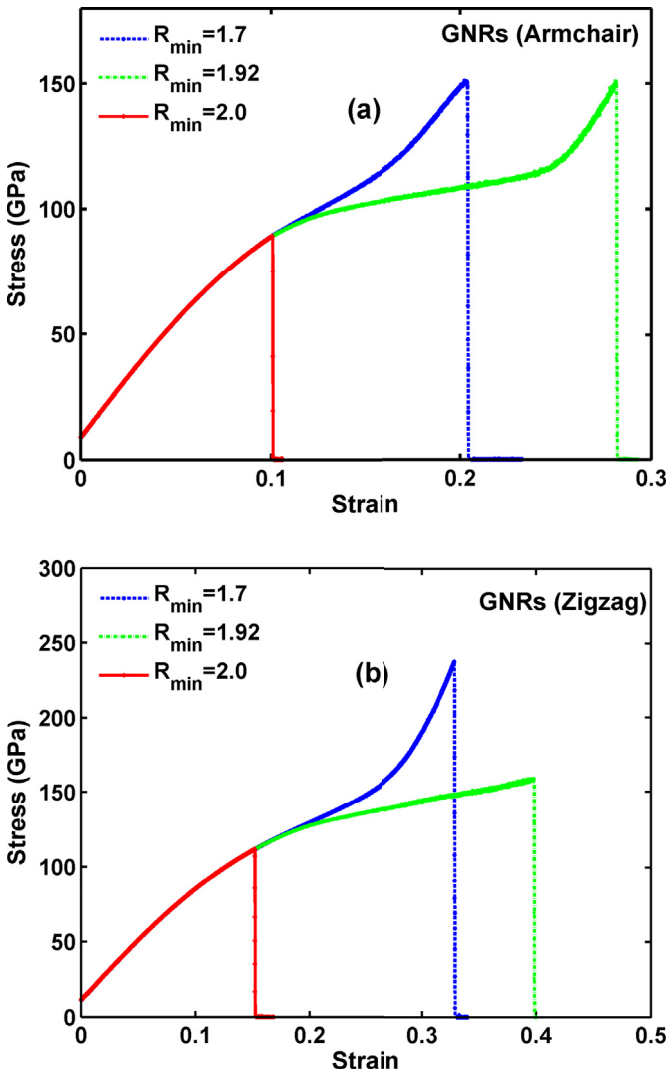

Fig. 2. Strain v.s. stress curves of GNRs using different R_{min}. (a) armchair GNRs; (b) zigzag GNRs.

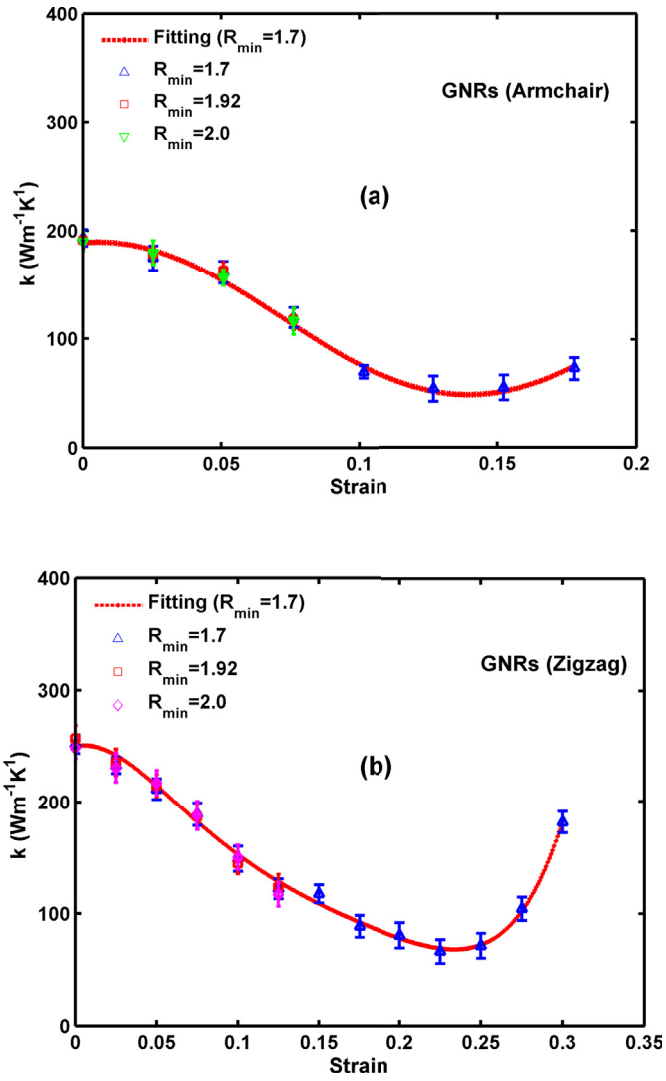

Fig. 3. Strain v.s. Thermal conductivity curves of GNRs using different R_{min}. (a) armchair GNRs; (b) zigzag GNRs.

conductivity under tensile strain and its transition point are a result from the overestimation of stress using the original AIREBO potential. The stage that the thermal conductivity increases with the applied strain corresponds to the second linearly elastic deformation part of the stress-strain curves of GNRs.

To understand the role of phonons in this anomalous heat conduction behavior, the phonon spectral density is calculated by Fourier transform of the velocity autocorrelation functions of the simulated systems. The phonon spectral density of the *ith* atom, $D_i(f)$, is defined as:

$$D_i(f) = \int \langle v_i(0) \cdot v_i(t) \rangle e^{-2\pi i f t} dt \tag{6}$$

where $v_i(t)$ is the velocity vector of the *ith* atom at time t and $\langle \cdots \rangle$ indicates an ensemble average.

Fig. 5(a) and (b) show the total phonon spectrum of the armchair and zigzag GNRs under different strain, respectively. It can be seen that the higher-frequency optical phonon modes (the primary peak of the phonon spectrum) are more sensitive to the axial strain than the lower-frequency modes. As shown in Fig. 5(a), for low strain level, $\varepsilon = 0$–0.15, the tension softens the G-bands remarkably in comparison with other part of the spectrum, and red shift of G-bands frequencies appears obviously, and thus lowers their group velocities and weakens the energy transfer. When $\varepsilon = 0.175$, the peak for G-band is blueshifted. In the phonon spectral density of zigzag GNRs shown in Fig. 5 (b), it can be seen that both redshift and blueshift of the peak for G-band are more obvious. For $\varepsilon = 0$–0.2, the G-bands of zigzag GNRs are redshifted; when $\varepsilon \geq 0.225$, the peak for G-band begins to blueshift, especially when $\varepsilon \geq 0.275$, the overestimation of stress (or Young's modulus) by the original AIREBO potential result in a flatter G-bands spectrum, and the frequency of the G-band are shifted to about 71.87 THz.

It has been reported that the heat conduction of CNTs and GNRs is dominated by the high-frequency modes, especially C—C characteristic peak. The variation of frequencies of the G-band of armchair and zigzag GNRs under different strains are shown in Fig. 6(a) and (b). Their variation trends and location of transition point have similar characteristics as those of thermal conductivity and the square root of the nominal modulus with respect to strain in Figs. 3 and 4. Besides, Fig. 7 shows the frequency of the G-band as a function of the square root of the nominal modulus of GNRs under different strains. It indicates that the frequency of the G-band is linear with the square root of the nominal modulus of GNRs.

We perform a two-dimensional Fourier transform of the atomic velocities to obtain the phonon spectral energy density and visualize the phonon dispersion relation. The power spectral maps for frequencies between 0 and 100 THz are analyzed for GNRs under different strains

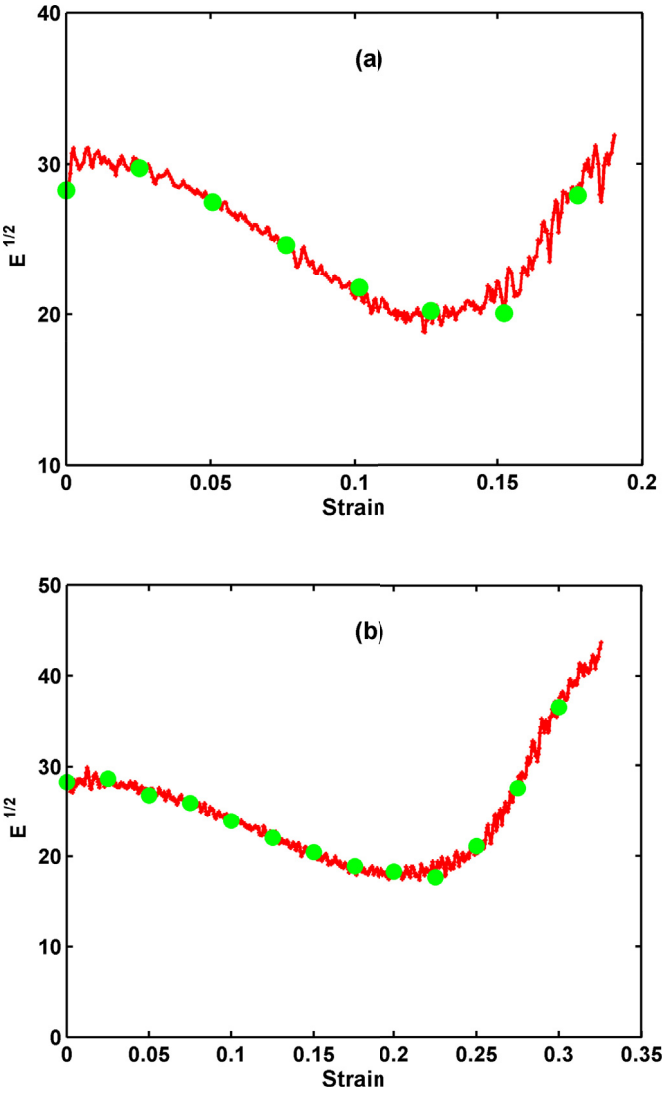

Fig. 4. The square root of the nominal modulus derived through differentiation of the stress with respect to strain. (a) armchair GNRs; (b) zigzag GNRs.

with ensemble averaged in 4096 sample windows. The phonon spectral energy density is calculated by Ref. [50].

$$\Phi(\omega,k)=\frac{1}{4\pi\tau_0 N_T}\sum_{\alpha}^{3}\sum_{b}^{B}m_b\left|\int_0^{\tau_0}\sum_{n_{x,y,z}}^{N_T}\left\{\dot{u}_\alpha\begin{pmatrix}n_{x,y,z}\\ b\end{pmatrix};t\right)\times\exp\left[ik\cdot r\begin{pmatrix}n_{x,y,z}\\ 0\end{pmatrix}-i\omega t\right]\right\}dt\right|^2 \tag{7}$$

Fig. 8(a), (b), (c) shows the phonon dispersion relations of zigzag GNRs under different strain $\varepsilon = 0$, 0.125, 0.3, respectively. Our result of phonon dispersion curves of GNRs for the case of $\varepsilon = 0$ using the AIREBO potential is in good agreement with previous studies [50,51]. It can be seen from Fig. 8 that the shift of lower-frequency phonon modes is small while the higher-frequency optical phonon modes (the primary peak of the phonon spectrum) are more sensitive to the axial strain than the lower-frequency modes.

For larger strain $\varepsilon = 0.125$, as shown in Fig. 8(b), the higher-frequency optical phonon modes are obviously depressed, and their phonon bands red-shift and the group velocity $v_g = \partial\omega/\partial k$ decreases as the strain increases, where ω and k is the corresponding frequency and

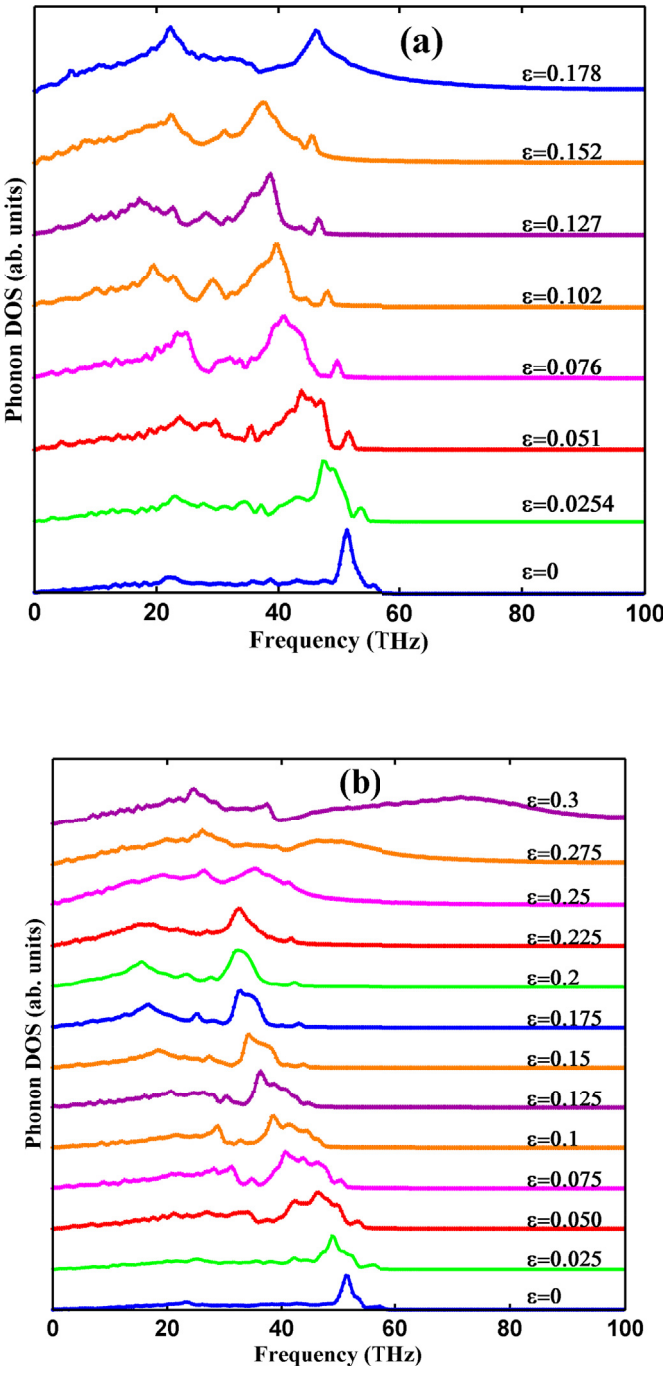

Fig. 5. Phonon spectra of GNRs under different strain: (a) armchair GNRs; (b) zigzag GNRs.

wavevector. However, for very large strain $\varepsilon = 0.3$ where the tensile strain almost approaches the failure limit, the effect is reverse; that is, higher-frequency optical phonon modes are dramatically blue-shifted, the optical phonon branches with higher frequency are obviously stiffened and the group velocity $v_g = \partial\omega/\partial k$ increases significantly while the scattering of the optical phonon modes are much more pronounced. The scattering of the optical phonon modes corresponds to the flatter G-bands spectrum as shown in Fig. 5(b). The peak-and-valley profiles along the entire frequency axis at a specific wave vector can be subtracted from the 3D map of the phonon spectral energy density. The peaks corresponding

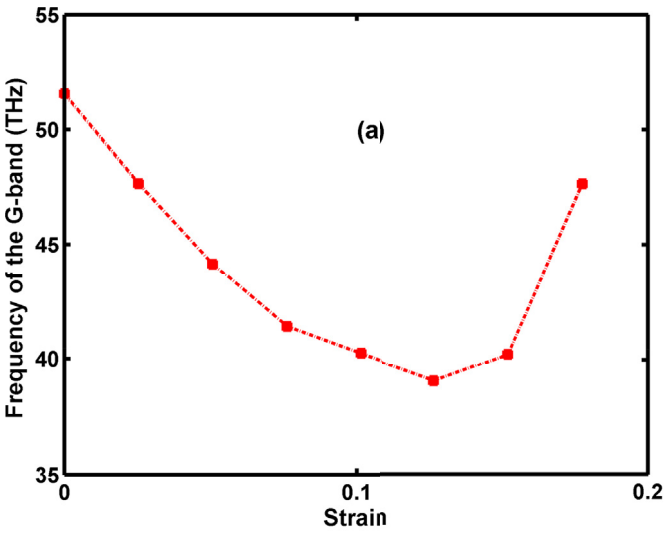

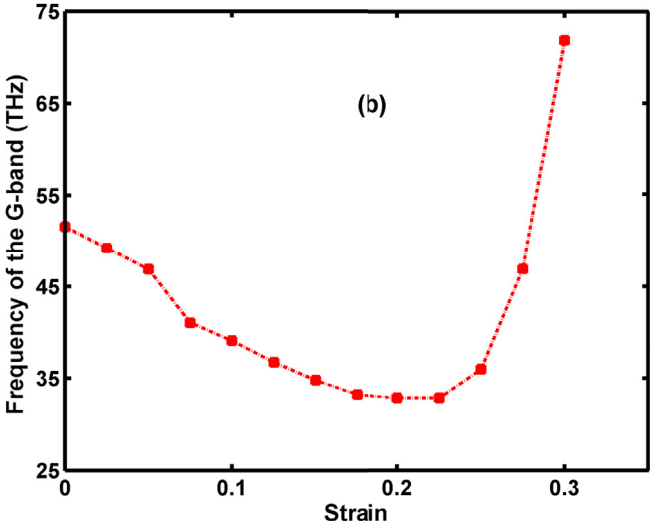

Fig. 6. Frequency of the G-band of GNRs under different strain: (a) armchair GNRs; (b) zigzag GNRs.

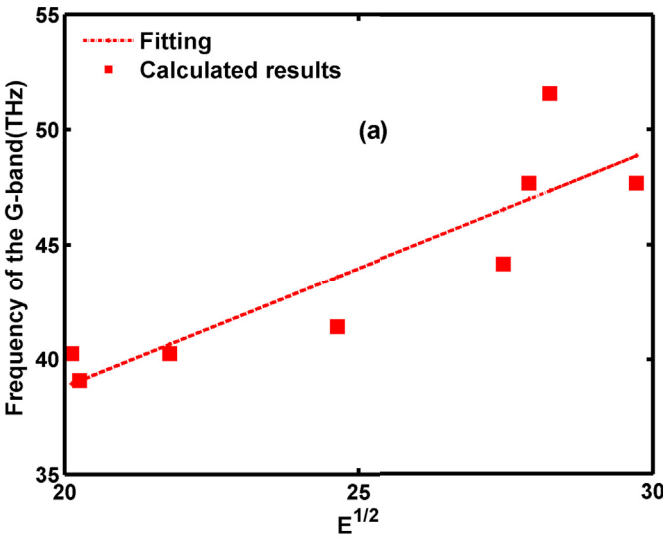

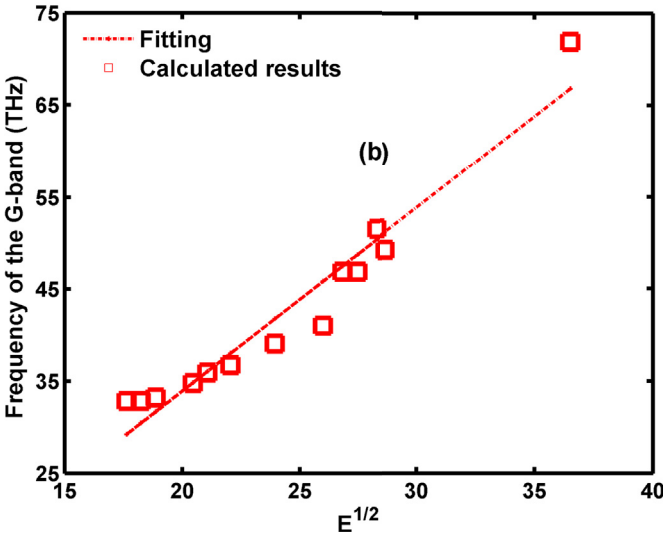

Fig. 7. Frequency of the G-band as a function of the square root of the nominal modulus of GNRs under different strain: (a) armchair GNRs; (b) zigzag GNRs.

to the scattered optical phonon branches with higher frequency have larger half-width at half-maximum and less phonon lifetime, thus can explain why the increase of the thermal conductivity of GRNs under extreme uniaxial strain are not so significant as that of the frequency of the G-band shown in Fig. 6 (b).

The thermal conductivity can be predicted by the classical lattice thermal transport theory, $k = \sum_m Cv_m l$, where C, v_m, l are the specific heat, group velocity and mean free path of phonon mode m. From the discussion above, the original AIREBO potential can provide good description of the thermal conductivity under normal conditions; however, for extreme deformation conditions, the original AIREBO potential gives an overestimation of the nominal modulus. This overestimation results in spurious phonon band structure, blue shift of G peak and phonon stiffening of the optical phonon modes, which artificially increase the group velocities in extreme strains near fracture. These results explain why the original AIREBO potential cause the spurious heat conduction behavior under extreme uniaxial strain that the thermal conductivity of GNRs does not monotonically decrease with increasing strain, and even shows a "V" shaped reverse, nonphysical trend.

4. Conclusions

In summary, the mechanical behavior and thermal transport of graphene nanoribbons (GNRs) are studied by MD simulations using both original and modified AIREBO potential. The key finding is that using the original AIREBO potential will result in artificial thermal phenomena and behavior at large strains on graphene nanoribbons. The important outcomes of our work are summarized below:

1) The original AIREBO potential result in an overestimated tunable range of strain in which thermal conductivity can be calculated.
2) The thermal conductivity of GNRs under tensile strain are significantly overestimated by the original AIREBO potential near the fracture stage during the tensile process, and even shows a "V" shaped reversed, nonphysical trend.
3) The cutoff function of the original AIREBO (REBO, Brenner) potential leads to serious overestimation for the thermal conductivity of GNRs when approaching fracture, and thus it should be modified when dealing with the cases of carbon nanostructures at large deformation.

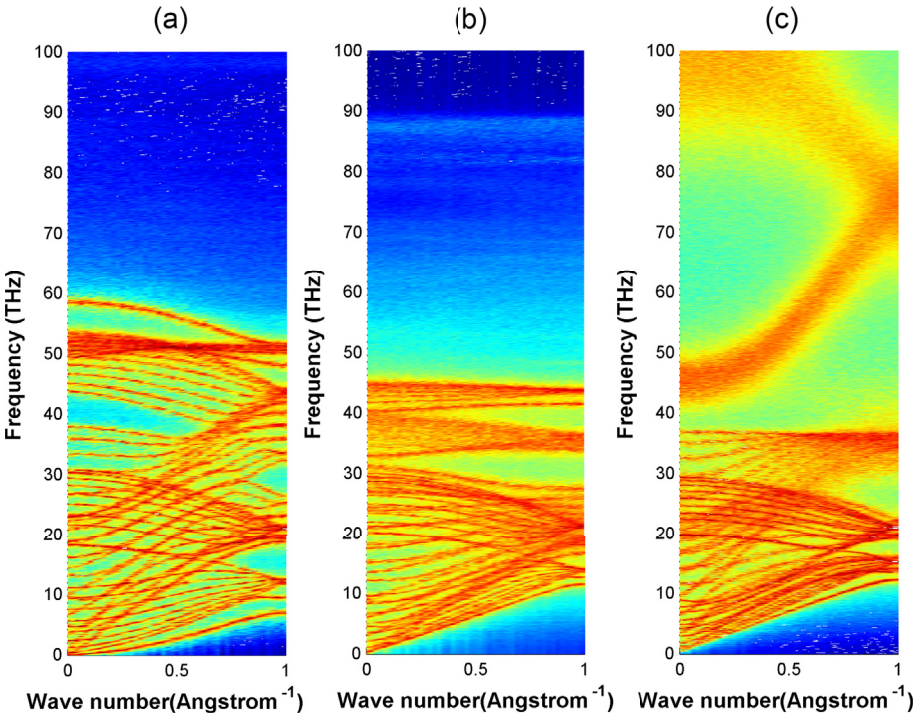

Fig. 8. Phonon band structure of zigzag GNRs calculated by the original AIREBO potential under different strain. (a) $\varepsilon = 0$; (b) $\varepsilon = 0.125$; (c) $\varepsilon = 0.3$.

For the modified AIREBO potentials, the modification of setting $R_{min} = 1.92$ Å cannot guarantee the full avoidance of nonphysical failures and the overestimation of mechanical properties of nanostructures near the fracture stage during the tensile process; the modified AIREBO with $R_{min} = 2.0$ Å is a more reasonable choice.

4) The origin of overestimation for thermal transport characterization of GNRs near the fracture stage during the tensile process is investigated. It shows that the camelback problem of the original AIREBO potential will lead to an artificial increase of Young's modulus, the blue shift of G peak and phonon stiffening of the optical phonon modes, resulting in an increase of group velocity of the phonons. Because the camelback problem also exists in Brener potential and REBO potential, such an overestimation problem by these potentials requires adequate attention.
5) The correlation between spurious heat conduction behavior and overestimation of mechanical properties in extreme strains near fracture caused by the original AIREBO potential are explored and revealed. The spurious heat conduction behaviors can be considered to be a result of the overestimation of the Young's modulus of GNRs using the original AIREBO potential. It indicates that the frequencies of the G-band are linear with the square root of the nominal modulus of GNRs.

Acknowledgments

This research is supported by the National Natural Science Foundation of China (Grant Nos. 51576066, 51322603, 51136001 and 51356001), the Natural Science Foundation of Hebei Province of China (Grant No. E2014502042).

References

[1] S. Bhowmick, V.B. Shenoy, J. Chem. Phys. 125 (2006) 164513.
[2] Z. Xu, J. Comput. Theor. Nanosci. 6 (2009) 625–628.
[3] S.K. Chien, Y.T. Yang, Carbon 50 (2012) 421–428.
[4] J.W. Jiang, B.S. Wang, J.S. Wang, Appl. Phys. Lett. 98 (2011) 113114.
[5] R. Faccio, P.A. Denis, H. Pardo, C. Goyenola, A.W. Mombrú, J. Phys. Condens. Matter 21 (2009) 285304.
[6] Z.Q. Ye, B.Y. Cao, W.J. Yao, T. Feng, X. Ruan, Carbon 93 (2015) 915–923.
[7] Y. Chu, T. Ragab, C. Basaran, Carbon 89 (2015) 169–175.
[8] K.G.S.H. Gunawardana, K. Mullen, J. Hu, Y.P. Chen, X. Ruan, Phys. Rev. B 85 (2012) 245417.
[9] R. Perriot, X. Gu, Y. Lin, V.V. Zhakhovsky, I.I. Oleynik, Phys. Rev. B 88 (2013) 064101.
[10] B.I. Yakobson, M.P. Campbell, C.J. Brabec, J. Bernholc, J. Comp. Mater. Sci. 8 (1997) 341–348.
[11] S.J. Stuart, A.B. Tutein, J.A. Harrison, J. Chem. Phys. 112 (2000) 6472–6486.
[12] M.Q. Chen, S.S. Quek, Z.D. Sha, C.H. Chiu, Q.X. Pei, Y.W. Zhang, Carbon 85 (2015) 135–146.
[13] A. Tabarraei, X. Wang, D. Jia, Comp. Mater. Sci. 121 (2016) 151–158.
[14] Y. Chu, T. Ragab, C. Basaran, Comput. Mater. Sci. 81 (2014) 269–274.
[15] M.A.N. Dewapriya, A.S. Phani, R.K.N.D. Rajapakse, Modell. Simul. Mater. Sci. Eng. 21 (2013) 065017.
[16] Z. Ozturk, C. Baykasoglu, M. Kirca, Int. J. Hydrogen Energ 41 (2016) 6403–6411.
[17] Y.Y. Zhang, Q.X. Pei, Y.W. Mai, Y.T. Gu, J. Phys. D. Appl. Phys. 47 (2014) 425301.
[18] O.A. Shenderova, D.W. Brenner, A. Omeltchenko, X. Su, L.H. Yang, Phys. Rev. B 61 (2000) 3877.
[19] T. Belytschko, S.P. Xiao, G.C. Schatz, R.S. Ruoff, Phys. Rev. B 65 (2002) 235430.
[20] S.J. Plimpton, J. Comput. Phys. 117 (1995) 1–19.
[21] D.W. Brenner, O.A. Shenderova, J.A. Harrison, S.J. Stuart, B. Ni, S.B. Sinnott, J. Phys. Condens. Mater 14 (2002) 783–802.
[22] S. Zhang, S.L. Mielke, R. Khare, D. Troya, R.S. Ruoff, G.C. Schatz, T. Belytschko, Phys. Rev. B 71 (2005) 115403.
[23] Y. Sun, K.M. Liew, Int. J. Numer. Methods. Eng. 75 (2008) 1238–1258.
[24] C. Jin, H. Lan, L. Peng, K. Suenaga, S. Iijima, Phys. Rev. Lett. 102 (2009) 205501.
[25] J.C. Meyer, C.O. Girit, M.F. Crommie, A. Zettl, Nature 454 (2008) 319–322. http://www.nature.com/nature/journal/v454/n7202/abs/nature07094.html - a1#a1.
[26] A. Chuvilin, J.C. Meyer, G. Algara-Siller, U. Kaiser, New J. Phys. 11 (2009) 083019.
[27] X. Yang, L. Wang, Y. Huang, Z. Han, A.C. To, Phys. Chem. Chem. Phys. 16 (2014) 21615–21619.
[28] X. Yang, L. Wang, Y. Huang, A.C. To, B.Y. Cao, Comp. Mater. Sci. 109 (2015) 49–55.
[29] X. Yang, Y. Huang, L. Wang, B. Cao, A.C. To, Mater. Des. 97 (2016) 86–92.
[30] M. Huhtala, A.V. Krasheninnikov, J. Aittoniemi, S.J. Stuart, K. Nordlund, K. Kaski, Phys. Rev. B 70 (2004) 045404.
[31] R. Grantab, V.B. Shenoy, R.S. Ruoff, Science 330 (2010) 946–948.
[32] M. Daly, C.V. Singh, J. Appl. Phys. 115 (2014) 223513.
[33] J. Gu, F. Sansoz, Carbon 66 (2014) 523–529.
[34] B.W. Jeong, J.K. Lim, S.B. Sinnott, Appl. Phys. Lett. 90 (2007) 023102.
[35] M. Sammalkorpi, A. Krasheninnikov, A. Kuronen, K. Nordlund, K. Kaski, Phys. Rev. B 70 (2004) 245416.
[36] H. Zhao, N.R. Aluru, J. Appl. Phys. 108 (2010) 064321.
[37] Y.J. Sun, Y.H. Huang, F. Ma, D.Y. Ma, T.W. Hu, K.W. Xu, Mater. Sci. Eng. B 180 (2014) 1–6.
[38] F. Zhu, H. Liao, K. Tang, Y. Chen, S. Liu, J. Nanomater 2015 (2015) 3.
[39] H. Zhao, K. Min, N.R. Aluru, Nano Lett. 9 (2009) 3012–3015.
[40] K. Mylvaganam, L.C. Zhang, Carbon 42 (2004) 2025–2032.
[41] W.C. Liu, F.Y. Meng, S.Q. Shi, Carbon 48 (2010) 1626–1635.
[42] Z. Guo, D. Zhang, X.G. Gong, Appl. Phys. Lett. 95 (2009) 163103.

[43] Z. Xu, M.J. Buehler, Nanotechnology 20 (2009) 185701.
[44] N. Wei, L. Xu, H.Q. Wang, J.C. Zheng, Nanotechnology 22 (2011) 105705.
[45] C. Lee, X. Wei, J.W. Kysar, J. Hone, Science 321 (2008) 385–388.
[46] Q.X. Pei, Y.W. Zhang, V.B. Shenoy, Carbon 48 (2010) 898–904.
[47] Y.Y. Zhang, Y. Cheng, Q.X. Pei, C.M. Wang, Y. Xiang, Phys. Lett. A 376 (2012) 3668–3672.
[48] X. Xu, L.F. Pereira, Y. Wang, J. Wu, K. Zhang, X. Zhao, et al., Nat. Commun. 1404 (2014) 5379.
[49] X. Li, K. Maute, M.L. Dunn, R. Yang, Phys. Rev. B 81 (2010) 245318.
[50] J.A. Thomas, J.E. Turney, R.M. Iutzi, C.H. Amon, A.J. McGaughey, Phys. Rev. B 81 (2010) 081411.
[51] J. Shiomi, S. Maruyama, Int. J. Thermophys. 31 (2010) 1945–1951.